

**Origins of the Enantioselectivity of Palladium Catalyst with
BINOL-Phosphoric Acid Ligands**

Journal:	<i>Organic & Biomolecular Chemistry</i>
Manuscript ID	OB-ART-09-2018-002271.R1
Article Type:	Paper
Date Submitted by the Author:	12-Oct-2018
Complete List of Authors:	Zhang, Jun; University of Illinois at Urbana-Champaign, Department of Chemistry



Cite this: DOI: 10.1039/xxxxxxxxxx

Origins of the Enantioselectivity of Palladium Catalyst with BINOL-Phosphoric Acid Ligands[†]

Jun Zhang^{*a}Received Date
Accepted Date

DOI: 10.1039/xxxxxxxxxx

www.rsc.org/journalname

Transition metal-catalyzed C–H activation with high enantioselectivity is a new and challenging field. BINOL-phosphoric acid ligands ((*R*)-TRIP) was found to be able to induce high enantioselectivity in aziridination of aliphatic amines by palladium-catalysis, and its origins are investigated in this study. We unveiled that in the effective catalyst, it is the acetate ligand rather than the phosphate that participates in assisting palladium catalysis due to its weaker Brønsted acidity. By comparison with the other two modified ligands, we demonstrate that the isopropyl groups of (*R*)-TRIP provide it extra degrees of freedom to affect the transition states leading to the *S* and *R* aziridination product in different ways. They create a roomy space for the acetate in the *S* transition state but raise a steric repulsion for it in the *R* transition state, making the former pathway much more favorable and achieving the enantioselectivity. This determination occurs entirely within the catalyst. This study deepens our understanding in transition metal-catalysis and provides new insights into the rational design of catalysts of high enantioselectivity.

1 Introduction

Activation of inert C–H bonds has been regarded as a challenging but promising field for various subjects in chemistry, like assembling large molecules^{1–4}, synthesis of natural products or pharmaceuticals^{5–8}, and C1 chemistry^{9–12}. Although metal-free catalysis is possible^{13–15}, currently transition metal (TM)-catalyzed activations are still the most ubiquitous.^{16–20} C–H amination is an important and efficient chemical process to construct *N*-functionalized compounds. Since the discovery of Mn-catalyzed C–H amination^{21,22}, catalysts containing TMs of group 7 to 11 have been developed for amination under mild conditions¹⁹. These reactions often involve a cyclometalation process²³. From these advances, palladium catalysts are recognized as having strong cyclometalation (i.e., cyclopalladation) tendency with aliphatic compounds, thus they can effect various kinds of C–H activations. Actually, since 2005²⁴, several palladium-catalyzed C–H aminations have been reported^{24–28}. An interesting example is shown in Figure 1a: palladium-catalysis (Pd(OAc)₂, **3**) of a tetramethyl substituted morpholinone **1**, through C–H activation, giving an aziridination product **2**²⁷. Such aziridination reactions are important in syntheses of pharmaceuticals, natural products, polymers, and organic materials¹⁹.

While the regioselectivity of C–H activation can often be real-

ized and understood^{23,29–32}, the achievement of high enantioselectivity is more challenging and has just attracted attention from chemical communities^{33–35}, because the required chiral ligands may not be active under the common reaction conditions needed for the TM-catalysis. Nevertheless, there are still many advances in enantioselective Pd-catalyzed C–H activations^{36–40}. For Fig. 1a, if a chiral 1,1'-binaphthol (BINOL)-phosphoric acid ligand, i.e., (*R*)-3,3'-bis(2,4,6-triisopropylphenyl)-1,1'-binaphthyl-2,2'-diyl hydrogen phosphate ((*R*)-TRIP), is introduced, under optimized reaction conditions (90 °C) in the solvent ethyl acetate (EtOAc), (*S*)-**2** will be the dominant product, achieving an enantiomeric ratio (e.r.) of 96.6:3.4 (Fig. 1b)⁴⁰. The effective catalyst in this reaction is **3TRIP** (Fig. 1c), where one acetate in **3** is substituted by (*R*)-TRIP. However, how the catalyst introduces enantioselectivity to the reaction still remains unclear. Understanding this is important for rational catalyst design for asymmetrical chemical syntheses. For this purpose, we reported herein a computational study on the origins of the enantioselectivity of this palladium-catalyzed aziridination reaction. Besides **3TRIP**, another two catalysts, **3HPA** and **3PhPA** (Fig. 1c), were also considered. The phosphate ligand of **3HPA** gained some early applications⁴¹, but nowadays its 3,3'-substitutions are more popular. It will be seen that a comparison of their catalytic properties can shed more lights on the catalytic process.

2 Computational Methods

The functional BLYP^{42,43} with Grimme DFT-D3 dispersion corrections⁴⁴ were used for all calculations. BLYP was selected because

^a Department of Chemistry, University of Illinois at Urbana–Champaign, Noyes Laboratory 355H 600 S. Mathews Ave. Urbana, IL 61801-3364, United States. E-mail: zhjun@illinois.edu

[†] Electronic Supplementary Information (ESI) available: Additional data and coordinates of molecules considered in this paper. See DOI: 10.1039/b000000x/

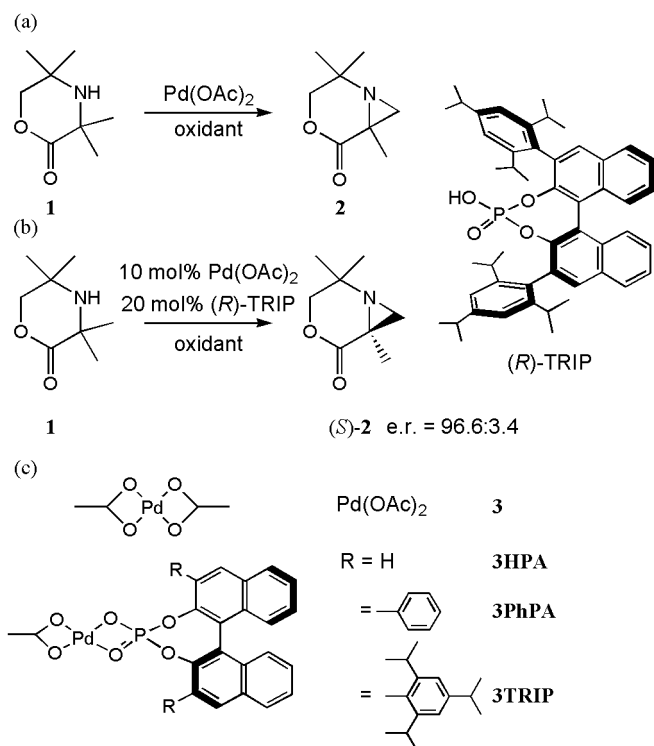


Fig. 1 (a) Nonenantioselective and (b) Enantioselective palladium-catalyzed C–H amination. (c) The effective catalysts considered in this study.

some hybrid functionals like B3LYP may predict unreasonable electronic structures for metallic complexes (like incorrect d orbital orders⁴⁵ or wrong ground states⁴⁶) while pure functionals often do much better. Also, the reliability of BLYP in palladium catalysis has been confirmed in several studies^{27,47,48}. DFT-D3 corrections are important since dispersion forces are known to be able to lead to an attractive interaction between the systems containing a large number of atoms or bulky functional groups⁴⁹, and such steric attractions can play a role in C–H activations⁵⁰. The EtOAc solvent environmental effects were accounted by the SMD solvation model^{51,52}. For nonmetallic elements and the valence electronic part of Pd, def2-TZVP basis set were applied⁵³. For Pd, its 28 core electrons were replaced by the Stuttgart-Cologne effective core potential⁵⁴. All the structures were optimized at the SMD(EtOAc)/BLYP-D3/def2-TZVP level of theory followed by a frequency calculation to check whether they were minima or transition states. The thermodynamics were calculated at 1 atm and 90 °C. The e.r. was estimated using

$$\text{e.r.} = \frac{\sum_{i=4\text{X-SOAc-TS}, 4\text{X-SPA-TS}} \exp(-\Delta G^\ddagger(i)/(RT))}{\sum_{i=4\text{X-ROAc-TS}, 4\text{X-RPA-TS}} \exp(-\Delta G^\ddagger(i)/(RT))} \quad (1)$$

where R is the gas constant and T is the absolute temperature (363.15 K). All quantum chemical calculations were carried out with Gaussian09D⁵⁵. The molecules and surfaces were rendered with CYLView 1.0b⁵⁶ and VMD 1.9.3⁵⁷.

3 Results and Discussions

The role of the catalyst, palladium(II) acetate, has been explored in detail²⁷. In the catalytic cycle, **1** will coordinate to **3** reversibly to produce intermediate **4**; then it undergoes the C–H activation, which also turns out to be the turnover-limiting step, through a transition state **4-TS**, to give a four-membered cyclopalladation species **5**. Then, after oxidation of **5** and some fast steps, the final product **2** is obtained and the catalyst is recovered (Fig. 2a).

For its enantioselective analog, at the first catalytic step, **3X** (X = HPA, PhPA, and TRIP) and **1** will give an intermediate **4X**, where N–H forms a dative bond with palladium and a hydrogen bond with an oxygen atom from **3X**. Now two scenarios are possible (Fig. 2b): N–H can form a hydrogen bond to either the phosphate or acetate; then the C–H activation will undergo through a transition state **4X-TS** using another ligand of palladium, i.e., the acetate or phosphate. Since Pd can only activate the methyl group that is syn to it, there are four scenarios for this stereocontrolling step: **SOAc/ROAc** and **SPA/RPA** (Fig. 2c. Here, **S/R** indicates that this intermediate is going to lead to the final product (**S/R**)-**2**; **OAc/PA** implies that it is the acetate/phosphate ligand of **3X** that engages directly in the C–H activation). Now one naturally raises two questions: (1) which scenario, **OAc** or **PA**, is more favorable, and (2) how the chirality of the phosphate ligand controls the preference of **S** and **R** scenario thus determines the final product.

3.1 Overview of the Scenarios

Using density functional theory (DFT), we can obtain the structures and energies of all the intermediates and transition states. The free energies of **4X** and **4X-TS** are shown in Fig. 3. For all **3X**'s, the activation free energies (ΔG^\ddagger) for **PA** scenarios are much higher than those for **OAc** scenarios. For **OAc** scenarios, in the order of X = HPA, PhPA, and TRIP, the relative stability between **4X-SOAc** and **4X-ROAc** approaches and then reverses, while the energy difference between **4X-SOAc-TS** and **4X-ROAc-TS** becomes more and more larger. This suggests that bulkier R groups can distinguish the transition states leading to products of different chirality better. Using ΔG^\ddagger 's in Fig. 3, e.r. can be estimated as 2.0:98.0, 2.2:97.8, and 99.99:0.01 for **3HPA**, **3PhPA**, and **3TRIP**, respectively, the last one being in good agreement with the experimental e.r. = 96.6:3.4⁴⁰. This suggests that bulkier R groups provides higher enantioselectivity as well as the reliability of our calculations. Now we will explore the chemical origins of the preference of these scenarios.

3.2 Preference of OAc or PA Scenarios

To better understand the catalytic processes, we have also performed a distortion/interaction analysis^{58,59} on the transition states, the results of which are given in Table 1 (a similar analysis for **4X** can be referred to Table S1). In this model, ΔE_{dist} corresponds to the energy difference that arises from structural changes during a chemical process and ΔE_{int} is the energy difference between **1** plus **3X** (both at distorted geometries) and **4X-TS**.

For the substrate **1**, its distortion energies $\Delta E_{\text{dist}}(\mathbf{1})$ in **PA** sce-

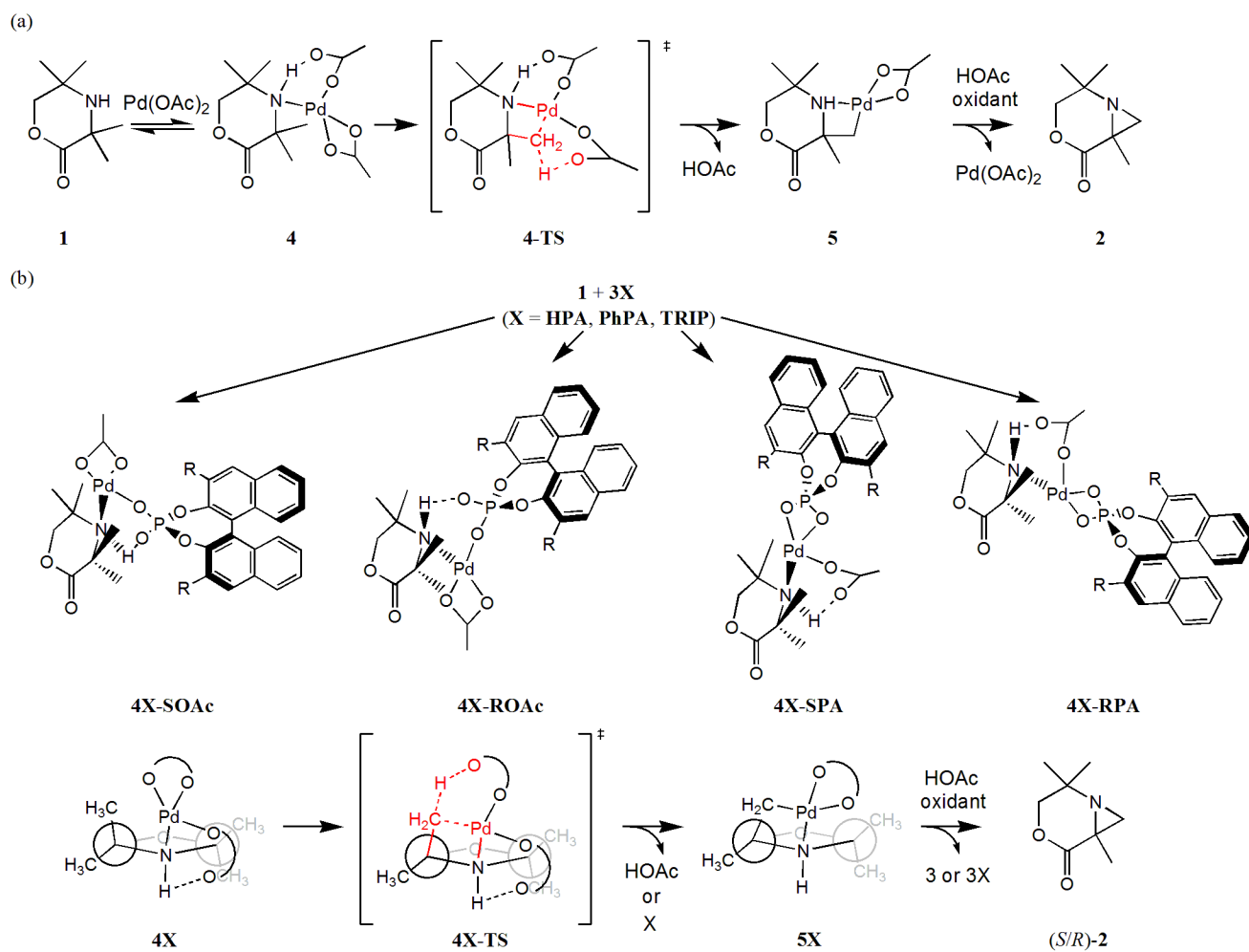


Fig. 2 The C–H activation step of the palladium-catalysis for (a) Fig. 1a and (b) Fig. 1b.

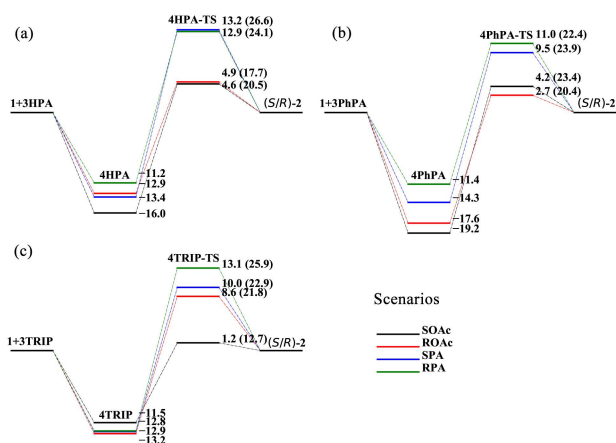


Fig. 3 The free energies of **4X** and **4X-TS** relative to separated reactants (ΔG) for all reaction scenarios. All energies are in kcal mol^{-1} . The numbers in parentheses are the activation free energies (ΔG^\ddagger).

Table 1 The distortion/interaction analysis for **4X-TS**. The energies are given in kcal mol^{-1} .

X and scenario	$\Delta E_{\text{dist}}(1)$	$\Delta E_{\text{dist}}(3X)$	$\Delta E_{\text{int}}(4X\text{-TS})$	$\Delta E(4X\text{-TS})$
4HPA-SOAc-TS	37.6	30.1	-79.4	-11.7
4HPA-ROAc-TS	38.2	30.1	-81.1	-12.8
4HPA-SPA-TS	53.0	33.9	-89.0	-2.1
4HPA-RPA-TS	52.9	34.3	-89.8	-2.6
4PhPA-SOAc-TS	36.4	28.2	-79.9	-15.3
4PhPA-ROAc-TS	39.1	28.4	-83.5	-16.0
4PhPA-SPA-TS	55.0	31.4	-91.8	-5.4
4PhPA-RPA-TS	53.6	32.7	-92.1	-5.8
4TRIP-SOAc-TS	38.5	29.6	-86.4	-18.3
4TRIP-ROAc-TS	42.9	33.2	-88.1	-12.0
4TRIP-SPA-TS	52.8	33.8	-93.1	-6.5
4TRIP-RPA-TS	52.8	35.7	-95.7	-7.2

narios are larger than those in **OAc** scenarios by more than 10 kcal mol^{-1} , in line with the observation revealed in Fig. 4 that the C–H bond to be activated is longer in **4X-PA-TS** than that in **4X-OAc-TS** by about 0.1 Å. This bond length increment contributes at least 10 kcal mol^{-1} to $\Delta E_{\text{dist}}(1)$ (See Fig. S1). Compared with other energy components, $\Delta E_{\text{dist}}(1)$ is the determining factor that leads to larger $\Delta E^\ddagger(4X\text{-TS})$ (as well as $\Delta G^\ddagger(4X\text{-TS})$) for **PA** scenarios, making them quite unfavorable.

The above discussion implies that in catalysts **3X**, the phosphate is weaker in assisting C–H activation than the acetate is, regardless of R group. This can be understood from their Brønsted acidities. The pK_a 's of acetate acid⁶⁰, **HPA**⁶¹, **PhPA**⁶¹, and **TRIP**⁶¹ are 12.3, 3.4, 3.9, and 5.1, respectively (all pK_a 's were measured in dimethyl sulfoxide. No data in EtOAc were found to the best of us⁶²), suggesting that the acetate is a much better proton acceptor than the phosphate is, in agreement with the fact that the calculated total electrostatic potential (ESP) is always larger at acetate oxygens than at phosphate ones in the same transition state (see Fig. 4 and Table S2) by up to 10 au. When palladium activates a methyl group, its d orbital will interact with the antibonding orbital of a C–H bond to weaken it (actually, as the hydrogen approaches the oxygen, the lone p pair of the latter also participates this weakening. See Scheme S1). As it elongates, a better proton acceptor, i.e., an oxygen atom with

higher ESP, can facilitate this process by offering it a favorable electrostatic environment to compensate the bond elongation energy penalty much better (see Fig. 5), making the reaction barrier occur earlier (shorter C–H bond in a transition state), leading to a smaller $\Delta E_{\text{dist}}(1)$ and thus smaller $\Delta E^\ddagger(4X\text{-TS})$ and $\Delta G^\ddagger(4X\text{-TS})$. Actually, natural bond orbital (NBO) analysis also suggested that the transition states in the **OAc** and **PA** scenarios are reactant- and product-like ones, respectively (see Scheme S1). Therefore, for all catalysts **3X**, the **OAc** scenario is believed to be main reaction channel.

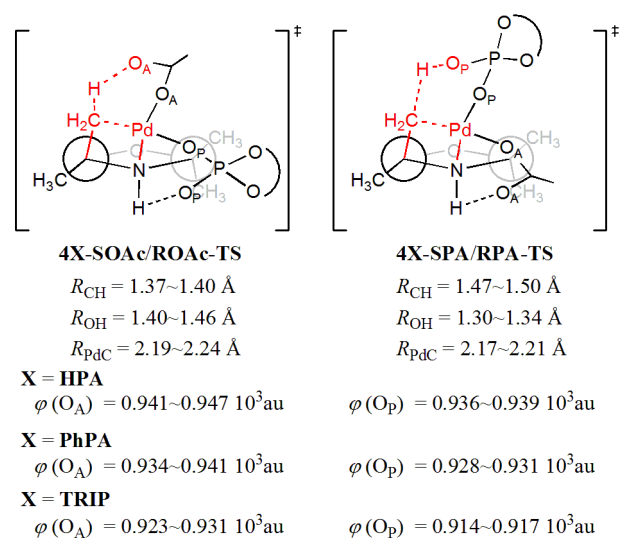


Fig. 4 Key geometrical and electronic parameters of the transition states **4X-TS**. For details see Table S2.

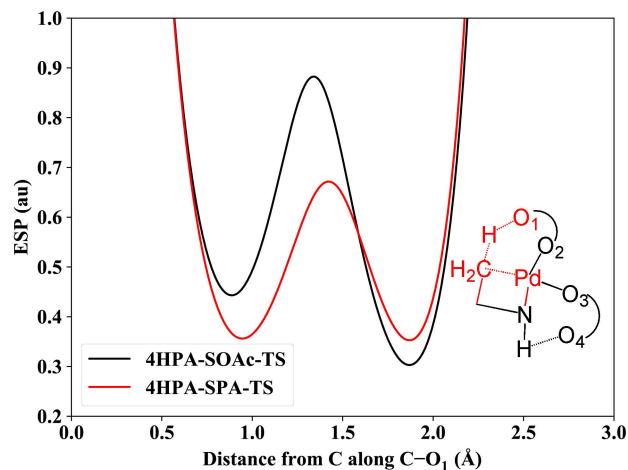


Fig. 5 Total electrostatic potential along C–O₁ path. For other transition states, the plots are similar.

3.3 Origins of the Enantioselectivity

The **S** or **R** scenario preference, i.e., the enantioselectivity of the reaction, will be explored for **OAc** scenarios here since **PA** scenarios are too unfavorable. This preference is determined by the relative stability of the species involved in the reaction. For ease

of notation, $\Delta\Delta E \equiv \Delta E(\text{in } 4\text{X-SOAc-TS}) - \Delta E(\text{in } 4\text{X-ROAc-TS})$ is defined here.

Because the essential C–H activation regions have similar geometrical parameters (like Pd–N, Pd–C, C–H, O–H, and hydrogen bond N–H...O–P) in **4X-OAc** or **4X-OAc-TS** (see Table S3), the enantioselectivity must originate from the catalysts. The geometries of **4TRIP-OAc** or **4TRIP-OAc-TS** are shown in Fig. 6, Fig. 7, and Fig. 8. We note that the Pd–N bond has to be *equatorial* in **4X-SOAc** and *axial* in **4X-ROAc**. This leads to a shorter distance between one acetate oxygen in **3X** and the ethyl oxygen of **1** in the latter (indicated by red wavy lines in Fig. 6. Please refer to Table S3 for details. Generally, about 5.6 Å in **4X-SOAc** versus 3.6 Å in **4X-ROAc**), raising a steric repulsion. Actually, this interprets the observation that **4HPA/4PhPA-SOAc** is more stable than their **ROAc** analogs (see Fig. 3. For **4X-TRIP-SOAc**, see below). In **4X-OAc-TS**, although all Pd–N's become axial, the bite angle between acetate and phosphate ($\angle\text{O}_2\text{-Pd-O}_3$ in Fig. 5) decreases, releasing this steric repulsion.

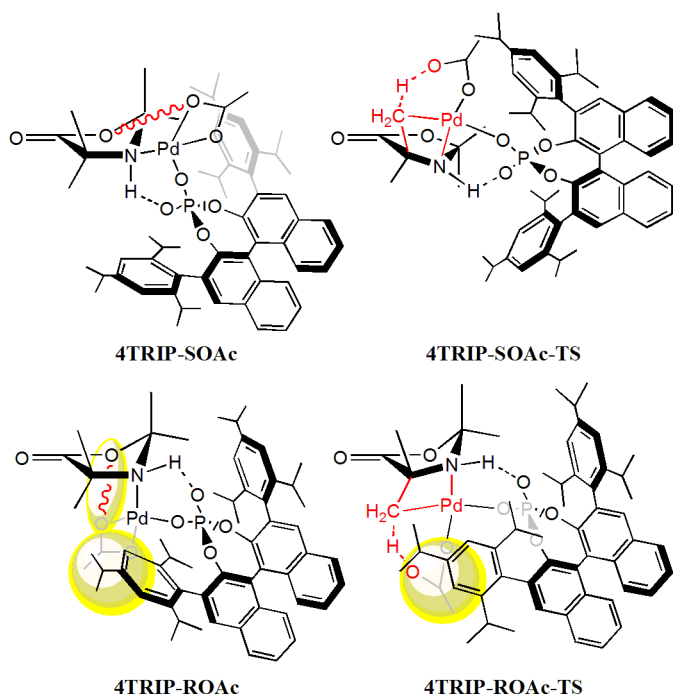


Fig. 6 The geometries of **4TRIP-OAc** and **4TRIP-OAc-TS**. The yellow circles indicate possible steric repulsions.

Table 1 reveals that $\Delta\Delta E_{\text{dist}}(\mathbf{1})$ is always negative. This seems to be a result of larger ring puckering in **4X-ROAc-TS** (see Table S3). Also, $\Delta\Delta E_{\text{int}}(\mathbf{4X-TS}) = +2.3 + 3.6 \text{ kcal mol}^{-1}$. At this stage, the total effect of $\Delta E_{\text{dist}}(\mathbf{1})$ and $\Delta\Delta E_{\text{int}}(\mathbf{4X-TS})$ will be supposed to lead to closely-lying **SOAc** and **ROAc** transition states for all catalysts. From **4X-OAc** to **4X-OAc-TS**, one Pd–O is broken and the acetate will rotate to assist C–H activation. In **SOAc** scenarios, the acetate will rotate more since Pd–N needs to change from the equatorial position to the axial one. For **3HPA** and **3PhPA**, we found that the potential energy surface of **3X** is rather flat with respect to the relative orientation of acetate and phosphate (see Figure S2), i.e., the acetate can rotate under small barrier within

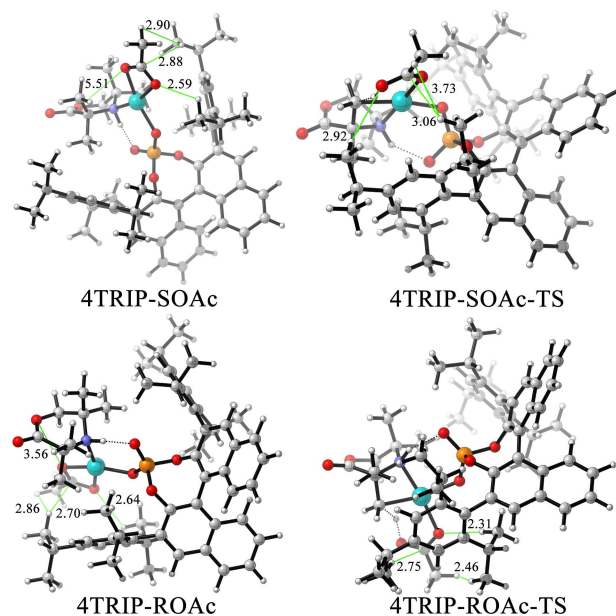


Fig. 7 The geometries of **4TRIP-OAc** and **4TRIP-OAc-TS**. Key nonbonding interactions (C–H, O–H, H–H, O–O) are rendered as green and the lengths are given in Å. There are considerable steric repulsions between the acetate and isopropyl groups in **4TRIP-ROAc-TS**.

the catalytic core. This interprets the interesting discovery that $\Delta\Delta E_{\text{dist}}(\mathbf{3X})$ for both are almost zero (less than $0.2 \text{ kcal mol}^{-1}$). Therefore, we can argue that **3HPA** and **3PhPA** determine the enantioselectivity only through delicate interaction difference in **SOAc** and **ROAc** scenarios, and the chirality of binaphthyl part of the catalyst is not *actively* involved in this determination.

This is different for **3TRIP**. The root mean square displacements (RMSDs) between **3X** in **4X-SOAc** and **4X-ROAc** for **X = HPA, PhPA, and TRIP** were calculated as 0.083 Å, 0.174 Å, and 0.928 Å, respectively. While **3HPA** and **3PhPA** have similar geometries in the two scenarios, the isopropyl groups of **3TRIP** show different poses in the two scenarios (see Figure S3), leading to a higher distortion energy (see Table S1). This counteracts the advantage of the absence of the oxygen repulsion mentioned above, making **4TRIP-SOAc** less stable. Actually, the lability of intermediate makes **3TRIP** more active. In the transition states, the relative orientation of acetate and phosphate in **X** is quite conserved in the **SOAc** and **ROAc** scenarios, respectively (see Fig. 7 and Fig. 8). However, in **4TRIP-ROAc-TS**, the acetate suffers from a strong steric repulsion from the isopropyl groups of the phosphate; in **4TRIP-SOAc-TS**, as Pd–N becomes axial, the acetate moves to a position that happens to be the crack of the catalyst, i.e., space between the isopropyl groups, enjoying a low repulsion environment and resulting in $\Delta\Delta E_{\text{dist}}(\mathbf{3TRIP}) = -3.6 \text{ kcal mol}^{-1}$ (see geometrical parameters in Fig. 7 and Fig. 8). Note that the atomic distances between isopropyl groups and acetate are in average 0.7 Å shorter in **4TRIP-ROAc-TS** than in **4TRIP-SOAc-TS**. This large $\Delta\Delta E_{\text{dist}}(\mathbf{3TRIP})$ makes the **SOAc** scenario much more favorable than the **ROAc** one: $\Delta\Delta G^\ddagger(\mathbf{4TRIP-OAc-TS}) = -9.1 \text{ kcal mol}^{-1}$ and e.r. = 99.99:0.01. **3TRIP** participates the entire stereocontrolling process *actively* by tuning energies and adjusting its

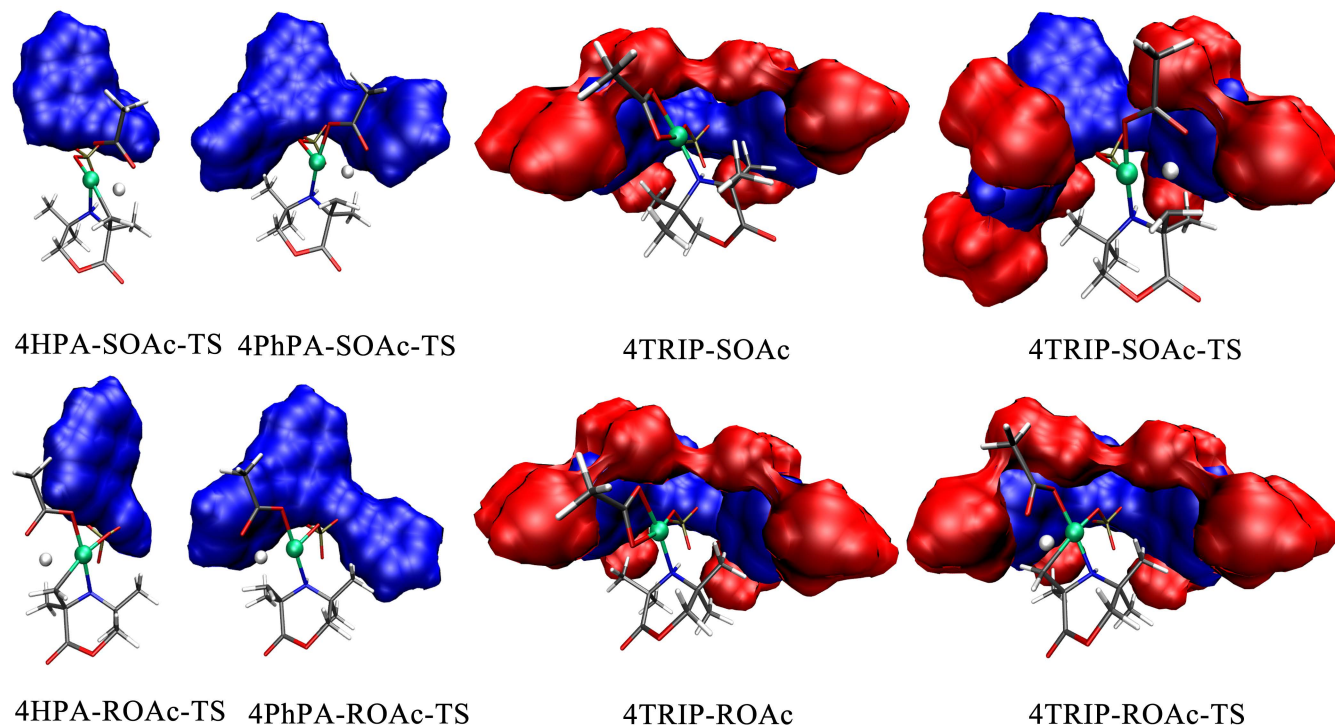


Fig. 8 The geometries of **4HPA-OAc-TS**, **4PhPA-OAc-TS**, **4TRIP-OAc**, and **4TRIP-OAc-TS**. Molecular surfaces for the 3,3'-biphenyl-1,1'-binaphthyl and isopropyl groups are rendered as blue and red, respectively.

conformations.

For highly enantioselective reactions, the transition states on the pathway leading to one enantiomer must be favored or disfavored for some reasons. In some cases like **3HPA** and **3PhPA**, it is a result of subtle interaction differences, which is difficult for a rational prediction of catalysis. Also, although their enantiomeric excess (*ee*) was theoretically estimated to be about 96%, its experimental value could be much smaller, since DFT studies of enantioselective reactions tend to overestimate *ee*^{63–66}. Both may cause their less popularity in chemical applications nowadays. In more interesting cases, the substrate will dock into a carefully designed catalyst (probably a rigid, supramolecular one) to achieve a high enantioselectivity^{67–71}. There are some specific interaction sites in the substrate that can bind to a recognition region of the catalyst (with, say, halogen or hydrogen bonds), and this pose usually allows the following functionalization occur only on one side of the prochiral plane.

It is another mechanism for **3TRIP**. Although it has the same catalytic core (palladium and Brønsted acid) and rigid backbone (*(R)*-3,3'-substituted-1,1'-binaphthyl) as **3HPA** and **3PhPA**, its substituents, i.e., 6 isopropyl groups, provide it with extra degrees of freedom to deform to fit specific chemical environments. They create a roomy space at the catalytic core in the **SOAc** scenario, but raise a steric repulsion in the **ROAc** scenario, therefore (*S*)-**2** becomes the dominant product. Such steric controllings are often observed between the catalyst and substrate^{72–79}, including some TRIP-catalyzed reactions^{75,76,79}. But for **3TRIP**, this enantioselectivity occurs within the catalyst. The similar pattern was observed in another Pd-catalyzed C–H activation reaction, where

the addition of mono-*N*-protected amino acids can induce enantioselectivity⁸⁰. Further study revealed that the steric repulsion between the isopropyl group of the amino acid and the *tert*-butyl group on the protecting ligand has a large impact on the reaction^{81,82}. Recently, an engineered iron-haem enzyme was synthesized and is able to catalyze C–H amination efficiently with high enantioselectivity⁸³. Inside the ligand pocket, the iron-haem activates C–H, and its approximal residues determine the stereochemistry. The isopropyl groups of **3TRIP** play a similar role in controlling reaction channels. Therefore, the enantioselectivity induced by intracatalyst interactions has analogs in enzymes and could be a useful rule for catalyst design.

4 Conclusions

We have thoroughly and successfully elucidated the origins of enantioselectivity in aziridination of aliphatic amines by palladium-catalyzed C–H activation with BINOL-phosphoric acid ligands (*(R)*-TRIP). The effective catalyst is Pd(OAc)((*R*)-TRIP) (**3TRIP**). Due to the weaker Brønsted acidity of acetate group than that of the phosphate group, the former can offer a better by offering it a beneficial electrostatic environment to facilitate the C–H activation, making the C–H bond length shorter by 0.1 Å and activation free energy lower by more than 10 kcal mol^{–1}, thus it is the acetate of **3TRIP** that engages directly in the C–H activation. By using distortion/interaction analyses and comparing with **3HPA** and **3PhPA**, we demonstrate that the isopropyl groups gives **3TRIP** more degrees of freedom to affect the transition states leading to *S* and *R* aziridination product in different ways. As the acetate of **3TRIP** adjusts to assist the C–H activa-

tion, isopropyl groups will hinder it in the *R* case, but form a roomy space for it in the *S* case (Fig. 7 and Fig. 8), leading to a high activation free energy thus achieving enantioselectivity. This enantioselective palladium catalysis involves both electronic and steric controlling. They can deepen our understanding of TM-catalysis and offer us new insights into rational design of catalysts of high enantioselectivity.

Conflicts of interest

There are no conflicts to declare.

Acknowledgements

J.Z. acknowledges Prof. So Hirata's support. J.Z. was supported by CREST, Japan Science and Technology Agency and by the Center for Scalable, Predictive methods for Excitation and Correlated phenomena (SPEC), which is funded by the U.S. Department of Energy (DOE), Office of Science, Office of Basic Energy Sciences, the Division of Chemical Sciences, Geosciences, and Biosciences.

References

- 1 J. Wencel-Delord and F. Glorius, *Nat. Chem.*, 2013, **5**, 369–375.
- 2 J. F. Hartwig and M. A. Larsen, *ACS Cent. Sci.*, 2016, **2**, 281–292.
- 3 Y.-J. Liu, Y.-H. Liu, Z.-Z. Zhang, S.-Y. Yan, K. Chen and B.-F. Shi, *Angew. Chem., Int. Ed.*, 2016, **55**, 13859–13862.
- 4 H. Fang, W. Hou, G. Liu and Z. Huang, *J. Am. Chem. Soc.*, 2017, **139**, 11601–11609.
- 5 J. Yamaguchi, A. D. Yamaguchi and K. Itami, *Angew. Chem., Int. Ed.*, 2012, **51**, 8960–9009.
- 6 P. E. Gormisky and M. C. White, *J. Am. Chem. Soc.*, 2013, **135**, 14052–14055.
- 7 Y. Y. See, A. T. Herrmann, Y. Aihara and P. S. Baran, *J. Am. Chem. Soc.*, 2015, **137**, 13776–13779.
- 8 R. R. Karimov, A. Sharma and J. F. Hartwig, *ACS Cent. Sci.*, 2016, **2**, 715–724.
- 9 J. Li, S. Zhou, J. Zhang, M. Schlangen, D. Usharani, S. Shaik and H. Schwarz, *J. Am. Chem. Soc.*, 2016, **138**, 11368–11377.
- 10 J. Li, S. Zhou, J. Zhang, M. Schlangen, T. Weiske, D. Usharani, S. Shaik and H. Schwarz, *J. Am. Chem. Soc.*, 2016, **138**, 7973–7981.
- 11 Y. Wang, X. Sun, J. Zhang and J. Li, *J. Phys. Chem. A*, 2017, **121**, 3501–3514.
- 12 H. Schwarz, S. Shaik and J. Li, *J. Am. Chem. Soc.*, 2017, **139**, 17201–17212.
- 13 M.-A. Légaré, M.-A. Courtemanche, É. Rochette and F.-G. Fontaine, *Science*, 2015, **349**, 513–516.
- 14 K. Chernichenko, M. Lindqvist, B. Kótai, M. Nieger, K. Sorochkina, I. Pápai and T. Repo, *J. Am. Chem. Soc.*, 2016, **138**, 4860–4868.
- 15 C. Tortoreto, D. Rackl and H. M. L. Davies, *Org. Lett.*, 2017, **19**, 770–773.
- 16 J. A. Labinger, *Chem. Rev.*, 2017, **117**, 8483–8496.
- 17 J. He, M. Wasa, K. S. L. Chan, Q. Shao and J.-Q. Yu, *Chem. Rev.*, 2017, **117**, 8754–8786.
- 18 R. Shang, L. Ilies and E. Nakamura, *Chem. Rev.*, 2017, **117**, 9086–9139.
- 19 Y. Park, Y. Kim and S. Chang, *Chem. Rev.*, 2017, **117**, 9247–9301.
- 20 Z. Dong, Z. Ren, S. J. Thompson, Y. Xu and G. Dong, *Chem. Rev.*, 2017, **117**, 9333–9403.
- 21 R. Breslow and S. H. Gellman, *J. Chem. Soc., Chem. Commun.*, 1982, 1400–1401.
- 22 R. Breslow and S. H. Gellman, *J. Am. Chem. Soc.*, 1983, **105**, 6728–6729.
- 23 T. Sperger, I. A. Sanhueza, I. Kalvet and F. Schoenebeck, *Chem. Rev.*, 2015, **115**, 9532–9586.
- 24 W. C. P. Tsang, N. Zheng and S. L. Buchwald, *J. Am. Chem. Soc.*, 2005, **127**, 14560–14561.
- 25 K. Sun, Y. Li, T. Xiong, J. Zhang and Q. Zhang, *J. Am. Chem. Soc.*, 2011, **133**, 1694–1697.
- 26 E. J. Yoo, S. Ma, T.-S. Mei, K. S. L. Chan and J.-Q. Yu, *J. Am. Chem. Soc.*, 2011, **133**, 7652–7655.
- 27 A. P. Smalley and M. J. Gaunt, *J. Am. Chem. Soc.*, 2015, **137**, 10632–10641.
- 28 D. Willcox, B. G. N. Chappell, K. F. Hogg, J. Calleja, A. P. Smalley and M. J. Gaunt, *Science*, 2016, **354**, 851–857.
- 29 B. A. Vastine and M. B. Hall, *Coord. Chem. Rev.*, 2009, **253**, 1202–1218.
- 30 D. Balcells, E. Clot and O. Eisenstein, *Chem. Rev.*, 2010, **110**, 749–823.
- 31 D. L. Davies, S. A. Macgregor and C. L. McMullin, *Chem. Rev.*, 2017, **117**, 8649–8709.
- 32 T. Gensch, M. J. James, T. Dalton and F. Glorius, *Angew. Chem., Int. Ed.*, 2012, **51**, 2296–2306.
- 33 H. M. L. Davies and R. E. J. Beckwith, *Chem. Rev.*, 2003, **103**, 2861–2904.
- 34 J.-Q. Yu, R. Giri and X. Chen, *Org. Biomol. Chem.*, 2006, **4**, 4041–4047.
- 35 T. G. Saint-Denis, R.-Y. Zhu, G. Chen, Q.-F. Wu and J.-Q. Yu, *Science*, 2018, **359**, year.
- 36 K.-J. Xiao, D. W. Lin, M. Miura, R.-Y. Zhu, W. Gong, M. Wasa and J.-Q. Yu, *J. Am. Chem. Soc.*, 2014, **136**, 8138–8142.
- 37 S.-B. Yan, S. Zhang and W.-L. Duan, *Org. Lett.*, 2015, **17**, 2458–2461.
- 38 K. S. L. Chan, H.-Y. Fu and J.-Q. Yu, *J. Am. Chem. Soc.*, 2015, **137**, 2042–2046.
- 39 H. Wang, H. Tong, G. He and G. Chen, *Angew. Chem., Int. Ed.*, 2016, **55**, 15387–15391.
- 40 A. P. Smalley, J. D. Cuthbertson and M. J. Gaunt, *J. Am. Chem. Soc.*, 2017, **139**, 1412–1415.
- 41 R. Noyori, K. Sato and Q. Yao, in *1,1'-Binaphthyl-2,2'-diyl Hydrogen Phosphate*, American Cancer Society, 2008.
- 42 A. D. Becke, *Phys. Rev. A*, 1988, **38**, 3098–3100.
- 43 C. Lee, W. Yang and R. G. Parr, *Phys. Rev. B*, 1988, **37**, 785–789.
- 44 S. Grimme, J. Antony, S. Ehrlich and H. Krieg, *J. Chem. Phys.*,

- 2010, **132**, 154104.
- 45 S. Patchkovskii, P. M. Kozłowski and M. Z. Zgierski, *J. Chem. Phys.*, 2004, **121**, 1317–1324.
- 46 P. Milko and M. A. Iron, *J. Chem. Theory Comput.*, 2014, **10**, 220–235.
- 47 J. Wassenaar, E. Jansen, W.-J. van Zeist, F. M. Bickelhaupt, M. A. Siegler, A. L. Spek and J. N. Reek, *Nat. Chem.*, 2010, **2**, 417–421.
- 48 L. P. Wolters, W.-J. van Zeist and F. M. Bickelhaupt, *Chem. Eur. J.*, 2014, **20**, 11370–11381.
- 49 J. Zhang and M. Dolg, *Chem. Eur. J.*, 2014, **20**, 13909–13912.
- 50 L. P. Wolters, R. Koekkoek and F. M. Bickelhaupt, *ACS Catal.*, 2015, **5**, 5766–5775.
- 51 A. V. Marenich, C. J. Cramer and D. G. Truhlar, *J. Phys. Chem. B*, 2009, **113**, 6378–6396.
- 52 R. F. Ribeiro, A. V. Marenich, C. J. Cramer and D. G. Truhlar, *J. Phys. Chem. B*, 2011, **115**, 14556–14562.
- 53 F. Weigend and R. Ahlrichs, *Phys. Chem. Chem. Phys.*, 2005, **7**, 3297–3305.
- 54 D. Andrae, U. Häußermann, M. Dolg, H. Stoll and H. Preuß, *Theor. Chim. Acta*, 1990, **77**, 123–141.
- 55 M. J. Frisch, G. W. Trucks, H. B. Schlegel, G. E. Scuseria, M. A. Robb, J. R. Cheeseman, G. Scalmani, V. Barone, B. Mennucci, G. A. Petersson, H. Nakatsuji, M. Caricato, X. Li, H. P. Hratchian, A. F. Izmaylov, J. Bloino, G. Zheng, J. L. Sonnenberg, M. Hada, M. Ehara, K. Toyota, R. Fukuda, J. Hasegawa, M. Ishida, T. Nakajima, Y. Honda, O. Kitao, H. Nakai, T. Vreven, J. A. Montgomery, Jr., J. E. Peralta, F. Ogliaro, M. Bearpark, J. J. Heyd, E. Brothers, K. N. Kudin, V. N. Staroverov, R. Kobayashi, J. Normand, K. Raghavachari, A. Rendell, J. C. Burant, S. S. Iyengar, J. Tomasi, M. Cossi, N. Rega, J. M. Millam, M. Klene, J. E. Knox, J. B. Cross, V. Bakken, C. Adamo, J. Jaramillo, R. Gomperts, R. E. Stratmann, O. Yazyev, A. J. Austin, R. Cammi, C. Pomelli, J. W. Ochterski, R. L. Martin, K. Morokuma, V. G. Zakrzewski, G. A. Voth, P. Salvador, J. J. Dannenberg, S. Dapprich, A. D. Daniels, O. Farkas, J. B. Foresman, J. V. Ortiz, J. Cioslowski and D. J. Fox, *Gaussian 09 Revision D.01*, Gaussian Inc. Wallingford CT 2009.
- 56 C. Y. Legault, *CYLview, 1.0b*, Université de Sherbrooke, 2009 (<http://www.cylview.org>).
- 57 W. Humphrey, A. Dalke and K. Schulten, *J. Mol. Graphics*, 1996, **14**, 33–38.
- 58 F. M. Bickelhaupt, *J. Comput. Chem.*, 1999, **20**, 114–128.
- 59 D. H. Ess and K. N. Houk, *J. Am. Chem. Soc.*, 2007, **129**, 10646–10647.
- 60 H. Bartnicka, I. Bojanowska and M. K. Kalinowski, 1991, **44**, 1077–1084.
- 61 P. Christ, A. G. Lindsay, S. S. Vormittag, J.-M. Neudörfl, A. Berkessel and A. C. O'Donoghue, *Chem. Eur. J.*, 2011, **17**, 8524–8528.
- 62 *Internet Bond-energy Databank (iBond) Home Page*: <http://ibond.chem.tsinghua.edu.cn> or <http://ibond.nankai.edu.cn>, An exhausted search has been done on iBond.
- 63 M. C. Holland, R. Gilmour and K. N. Houk, *Angew. Chem., Int. Ed.*, 2016, **128**, 2062–2067.
- 64 T. Lee and J. F. Hartwig, *J. Am. Chem. Soc.*, 2017, **139**, 4879–4886.
- 65 F. W. van der Mei, C. Qin, R. J. Morrison and A. H. Hoveyda, *J. Am. Chem. Soc.*, 2017, **139**, 9053–9065.
- 66 M. Li, X.-S. Xue and J.-P. Cheng, *ACS Catal.*, 2017, **7**, 7977–7986.
- 67 A. Bauer, F. Westkämper, S. Grimme and T. Bach, *Nature*, 2005, **436**, 1139.
- 68 P. Dydio, C. Rubay, T. Gadzikwa, M. Lutz and J. N. H. Reek, *J. Am. Chem. Soc.*, 2011, **133**, 17176–17179.
- 69 P. Fackler, S. M. Huber and T. Bach, *J. Am. Chem. Soc.*, 2012, **134**, 12869–12878.
- 70 J. Daubignard, R. J. Detz, A. C. H. Jans, B. de Bruin and J. N. H. Reek, *Angew. Chem., Int. Ed.*, 2017, **56**, 13056–13060.
- 71 F. Burg, M. Gicquel, S. Breitenlechner, A. Pöthig and T. Bach, *Angew. Chem., Int. Ed.*, 2018, **57**, 2953–2957.
- 72 E. Larionov, M. Nakanishi, D. Katayev, C. Besnard and E. P. Kundig, *Chem. Sci.*, 2013, **4**, 1995–2005.
- 73 Y. Dang, S. Qu, Z.-X. Wang and X. Wang, *J. Am. Chem. Soc.*, 2014, **136**, 986–998.
- 74 K. Kubota, M. Jin and H. Ito, *Organometallics*, 2016, **35**, 1376–1383.
- 75 Y. Y. Khomutnyk, A. J. Argüelles, G. A. Winschel, Z. Sun, P. M. Zimmerman and P. Nagorny, *J. Am. Chem. Soc.*, 2016, **138**, 444–456.
- 76 R. N. Straker, Q. Peng, A. Mekareeya, R. S. Paton and E. A. Anderson, *Nat. Comm.*, 2016, **7**, 10109.
- 77 B. Tutkowski, E. Meggers and O. Wiest, *J. Am. Chem. Soc.*, 2017, **139**, 8062–8065.
- 78 H. Suga, Y. Hashimoto, Y. Toda, K. Fukushima, H. Esaki and A. Kikuchi, *Angew. Chem., Int. Ed.*, 2017, **56**, 11936–11939.
- 79 J. P. Reid and J. M. Goodman, *Chem. Eur. J.*, 2017, **23**, 14248–14260.
- 80 B.-F. Shi, N. Mangel, Y.-H. Zhang and J.-Q. Yu, *Angew. Chem. Int. Ed.*, 2008, **47**, 4882–4886.
- 81 D. G. Musaev, A. Kaledin, B.-F. Shi and J.-Q. Yu, *J. Am. Chem. Soc.*, 2012, **134**, 1690–1698.
- 82 G.-J. Cheng, P. Chen, T.-Y. Sun, X. Zhang, J.-Q. Yu and Y.-D. Wu, *Chem. Eur. J.*, 2015, **21**, 11180–11188.
- 83 C. K. Prier, R. K. Zhang, A. R. Buller, S. Brinkmann-Chen and F. H. Arnold, *Nat. Chem.*, 2017, **9**, 629.